

Bending performance of concrete beams retrofitted with mechanochromic glass/carbon hybrid composites

Combining structural reinforcement and visual health monitoring

Mohammadi, Reza; Fathi, Ahmad; Schlangen, Erik; Fotouhi, Mohammad

DOI

[10.1016/j.conbuildmat.2024.139597](https://doi.org/10.1016/j.conbuildmat.2024.139597)

Publication date

2025

Document Version

Final published version

Published in

Construction and Building Materials

Citation (APA)

Mohammadi, R., Fathi, A., Schlangen, E., & Fotouhi, M. (2025). Bending performance of concrete beams retrofitted with mechanochromic glass/carbon hybrid composites: Combining structural reinforcement and visual health monitoring. *Construction and Building Materials*, 458, Article 139597. <https://doi.org/10.1016/j.conbuildmat.2024.139597>

Important note

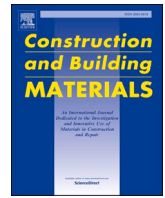
To cite this publication, please use the final published version (if applicable). Please check the document version above.

Copyright

Other than for strictly personal use, it is not permitted to download, forward or distribute the text or part of it, without the consent of the author(s) and/or copyright holder(s), unless the work is under an open content license such as Creative Commons.

Takedown policy

Please contact us and provide details if you believe this document breaches copyrights. We will remove access to the work immediately and investigate your claim.



Bending performance of concrete beams retrofitted with mechanochromic glass/carbon hybrid composites: Combining structural reinforcement and visual health monitoring

Reza Mohammadi ^a, Ahmad Fathi ^b, Erik Schlangen ^a, Mohammad Fotouhi ^{a,*} 

^a Faculty of Civil Engineering and Geosciences, Delft University of Technology, Delft CD 2628, the Netherlands

^b Department of Civil Engineering, University of Minho, Guimarães 4800-058, Portugal

ARTICLE INFO

Keywords:

Mechanochromic composite
Flexural BEHAVIOUR
Externally Bonded Reinforcement (EBR)
Structural Health Monitoring (SHM)
Retrofitting
Self-reporting composite

ABSTRACT

This study evaluates the performance of damaged concrete beams retrofitted with a purpose-designed mechanochromic composite, which provides structural reinforcement and visual feedback for structural health monitoring (SHM). The retrofitting process utilizes externally bonded reinforcement (EBR) on pre-damaged concrete prisms. The mechanochromic composite, a thin-ply hybrid material made of unidirectional ultra-high modulus (UHM) carbon/epoxy and S-glass/epoxy layers, changes color to indicate structural overload when the UHM carbon layer fractures due to excessive strain. Eighteen concrete specimens were prepared and subjected to four-point bending tests, assessing various combinations of damaged, undamaged, retrofitted, and non-retrofitted configurations. Results showed that the mechanochromic composite functions effectively as both a passive visual sensor and reinforcement. For instance, a 5 % crack depth reduced load-bearing capacity by 30 %, however, retrofitting with the mechanochromic composite improved load-bearing capacity by up to 208 % compared to undamaged beams. The study further discusses the effects of different damage levels on load-bearing capacity through flexural strength, load-displacement curves, and failure modes.

1. Introduction

Many structures over the world are categorized as having critical load-bearing capacity due to the degradation of their structural and mechanical properties over time. This weakening can result from factors such as ageing, corrosion, changes in the magnitude and direction of applied loads and other influences [1–4]. To overcome this issue, various strengthening methods have been developed over the past few decades to repair these structures and extend their service life. One of the earliest solutions was the replacement of the structural member itself; however, the high costs, complexity of the implementation, and sustainability issues associated with this method led to its substitution with more practical techniques, such as repairing structural members by mounting external materials like steel plates or composites [5,6].

Composites have been widely used for retrofitting various types of concrete structural members such as walls, beams, columns, and vaults taking advantage of two primary techniques, namely near surface mounted (NSM) and externally bonded reinforcement (EBR) methods [7–9]. In the first technique, composite materials, typically in the form

of rods or bars, are bounded into pre-cut grooves within the structural element. This approach is particularly effective in conditions where aesthetics or protection of the reinforcement is a concern, as the composite is embedded within the structural element [10–12]. On the other hand, the EBR method involves attaching the composite materials, such as fiber-reinforced polymers (FRPs), directly to the surface of the structural element utilizing mechanical anchors or adhesives [13,14]. EBR has gained popularity due to its simplicity and flexibility in application, making it suitable for a wide range of structures and damage scenarios [15,16]. While both methods have been extensively used and provide notable benefits, they also have certain limitations. NSM reinforcement is more resistant to environmental degradation due to its embedded nature, but its implementation can be more complicated, costly, and time-consuming [17–19]. Conversely, EBR is easier and faster to apply, especially for large surface areas, but it may be more vulnerable to environmental factors such as moisture or UV exposure, which could affect the durability of the bond between the composite and the substrate [20]. Despite these limitations, both approaches have proven influential in improving the structural performance and

* Corresponding author.

E-mail address: m.fotouhi-1@tudelft.nl (M. Fotouhi).

<https://doi.org/10.1016/j.conbuildmat.2024.139597>

Received 28 September 2024; Received in revised form 17 November 2024; Accepted 13 December 2024

Available online 17 December 2024

0950-0618/© 2024 The Author(s). Published by Elsevier Ltd. This is an open access article under the CC BY license (<http://creativecommons.org/licenses/by/4.0/>).

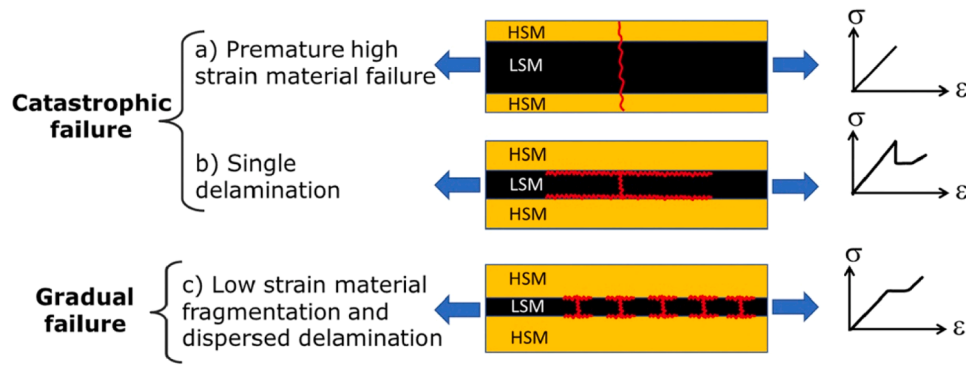


Fig. 1. Illustration of various failure modes in a three-layer, unidirectional hybrid laminate made of high-strain and low-strain materials, with red lines marking the fractures. The scenarios depicted include: (a) a single fracture spanning the entire specimen; (b) a single fracture occurring solely in the low-strain material, leading to immediate delamination; and (c) numerous fractures accompanied by a stable, localized pull-out within the low-strain material [30].

extending the service life of various infrastructure elements.

Retrofitted areas that pass routine visual inspection can fail under unexpectedly low loads, making it essential to monitor their integrity and detect damage early (if there is any). Researchers have employed various methods to monitor retrofitted structures for maintenance and to mitigate the risk of unexpected failure. Timely detection prevents sudden failures, enables targeted non-destructive testing, and ensures necessary repairs or maintenance, minimizing downtime and extending service life. A key advantage of the EBR technique is its ease of implementation and its greater potential for integrating real-time Structural Health Monitoring (SHM) systems. Current SHM techniques include Acoustic Emission (AE) [21,22], ultrasonic methods [23,24], and infrared thermography [25]. These SHM solutions for retrofitted areas in concrete structures often rely on expensive equipment, electrical power, complex data acquisition systems, and skilled operators, making them costly and impractical for long-term use.

To address this research gap, this study introduces, for the first time, the integration of self-reporting functionality into FRPs using mechanochromic hybrid composites. These mechanochromic hybrid composites offer a cost-effective and durable monitoring solution, capable of providing long-term, reliable performance without the need for complex systems or external power sources. These composites change colour in response to mechanical deformation [26]. This allows for real-time, wireless, and power-free monitoring of the structure without the need for complex data acquisition systems, further data analysis, external power sources, or expert operators [27].

The use of mechanochromic composites represents a significant advancement for SHM, particularly in structures where access is limited,

or continuous electrical monitoring is not practical. By providing immediate visual feedback, these materials can act as early warning systems, offering potential for safer operation in service. This is especially valuable in critical infrastructure, such as bridges, tunnels, and dams, where the consequences of undetected structural damage can be severe. Additionally, the application of such smart materials aligns with the growing emphasis on sustainable construction practices, as it reduces the need for frequent inspections and invasive testing, thereby minimizing the structure's lifecycle costs and environmental impact.

Thin-ply hybrid composite sensors are designed for a straightforward application, providing a visual alert of an overload taking advantage of a fracture-triggered sensing mechanism. As can be seen in Fig. 1, they are composed of commercial preregs and experience different failure mechanisms within a multi-layer unidirectional hybrid laminate made with low- and high-strain materials. The translucent nature of the high-strain material (glass-epoxy layers) provides visual cues to the naked eye, revealing the fracture of the low-strain material (carbon-epoxy layers) and delamination between the carbon and glass layers. The rationale behind their design is to ensure a visual alert to strain overload by visually readable distributed delamination and the fracture of low-strain material as per Fig. 1C. For this purpose, the properties of the materials and the thickness ratios between low- and high-strain materials need to be selected carefully [28]. A combination of these thin-ply hybrid composites and EBR technique can result in self-reporting retrofitting solutions both for SHM and reinforcement purposes [29], eliminating the need for electrical-based SHM sensors to evaluate the structural integrity of the retrofitted areas.

The implementation of mechanochromic thin-ply hybrid composite



Fig. 2. Curing of the concrete prisms: (a) under plastic sheets, before unmoulding; and (b) in the moisture chamber, after unmoulding.

Table 1

The selected plan for experimental tests.

Group name	Label	Crack Depth (mm)	Damage (%)	Retrofitted?	Number of prisms	Label of prisms
Reference	REF	-	0	No	3	C1, C2, C3
5 % damage	LD	5	5	No	3	LD1, LD2, LD3
15 % damage	HD	15	15	No	3	HD1, HD2, HD3
5 % damage + retrofitting	RLD	5	5	Yes	3	RLD1, RLD2, RLD3
15 % damage + retrofitting	RHD	15	15	Yes	3	RHD1, RHD2, RHD3

as a reinforcement material and its ability to recover the load-bearing capacity of the damaged element are investigated in this paper. For this, a series of pre-damaged concrete prisms were retrofitted using this composite and their performance was monitored in the form of failure mode, load-bearing capacity, and load-displacement curves by subjecting the prisms to a four-point bending test.

2. The preparation of concrete prisms

The specimens were produced using a uniform concrete mixture. The mix proportions by weight were cement: water: sand: gravel = 1:0.42:1.4:2.50. Crushed limestone that passed through a 15 mm sieve served as the coarse aggregate, while natural river sand with a fineness modulus of 2.3 was used as the fine aggregate. The steel molds have been used for casting process. The dimensions of the prisms are $10 \times 10 \times 40 \text{ cm}^3$. After curing all the prisms under a relative humidity of 95 % for a period of 28 days, under plastic sheets for the first 24 hours, before un moulding, (Fig. 2-A) and in a moisture room for the

next 27 days (Fig. 2-B), all of them were taken out of the room for further preparation prior to testing including cutting the grooves and retrofitting.

A series of fifteen specimens with varying levels of damage, both with and without retrofitting, were subjected to a standard 4-point bending test. These specimens were categorized into five groups, each consisting of three prisms. As detailed in Table 1: (a) the undamaged and non-retrofitted group, referred to as the REF group; (b) the group with 5 % light damage and no retrofitting, termed the LD group; (c) the group with 5 % damage and retrofitted, named the RLD group; (d) the group with 15 % heavy damage and no retrofitting, known as the HD group; and (e) the group with 15 % damage and retrofitted, identified as the RHD group. Additionally, three cubic specimens (with dimension of $10 \times 10 \times 10 \text{ cm}^3$) were cast for compression testing to determine the compressive strength and Young's modulus.

3. Retrofitting by hybrid composite

The mechanochromic EBR composite is a thin-ply hybrid composite consisting of one layer of unidirectional S-glass/epoxy and another layer of unidirectional ultra-high modulus YSH-90 carbon/epoxy, with a Young's modulus of 800 GPa. The composition of the EBR was chosen carefully to ensure that under loading condition, the layers designed to bear low strain would not fail. Instead, overloading would trigger fibre failure in these low strain sensor materials, leading to a visible change in appearance. Furthermore, the use of materials with higher moduli for the patch facilitates a more effective and rapid redistribution of load from the damaged panel to the EBR composite patch. This patch was developed as an initial demonstration of the concept. The decision to use YSH-90 fiber prepreg was due to the low strain to failure of 0.3 %, making it sensitive to low strain levels for sensing [9]. For the high strain component, S-glass prepregs were selected due to their strength and stiffness, with a longitudinal modulus of 45.6 GPa and a failure strain exceeding 4 %. Before retrofitting, the concrete surface was thoroughly cleaned and then sanded with sandpaper to ensure strong adhesive bonding between the concrete and the composite. During the lamination process, the first five layers of S-glass prepreg were applied by hand as

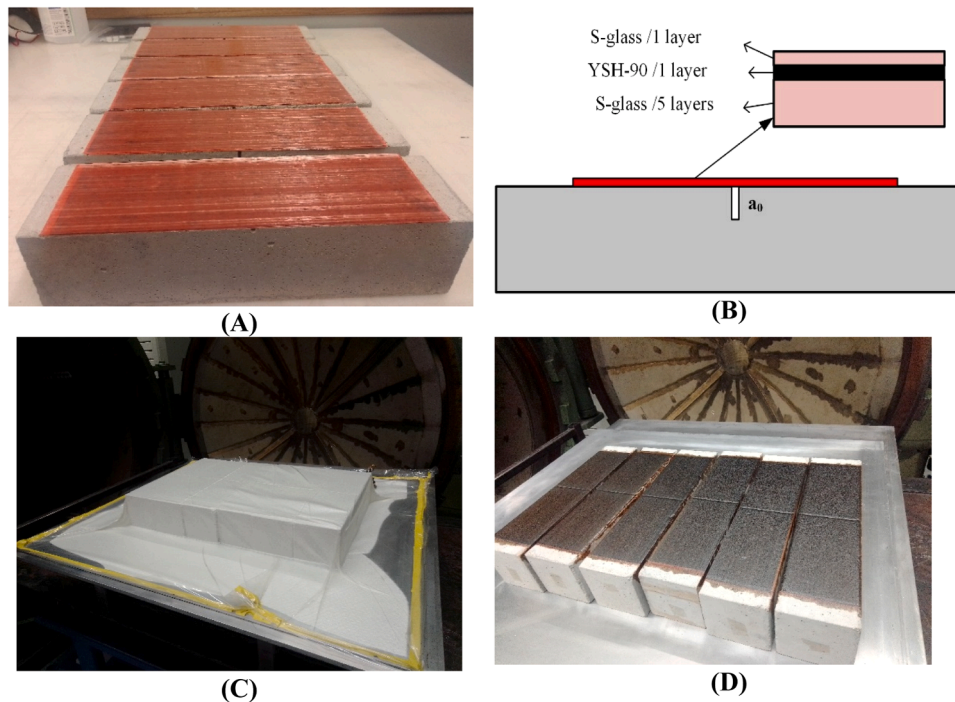


Fig. 3. Retrofitting process with hybrid composite: (A) lamination process (B) Schematic of sequence layers (C) Vacuum process (D) Retrofitted specimens after curing and unmolding process.



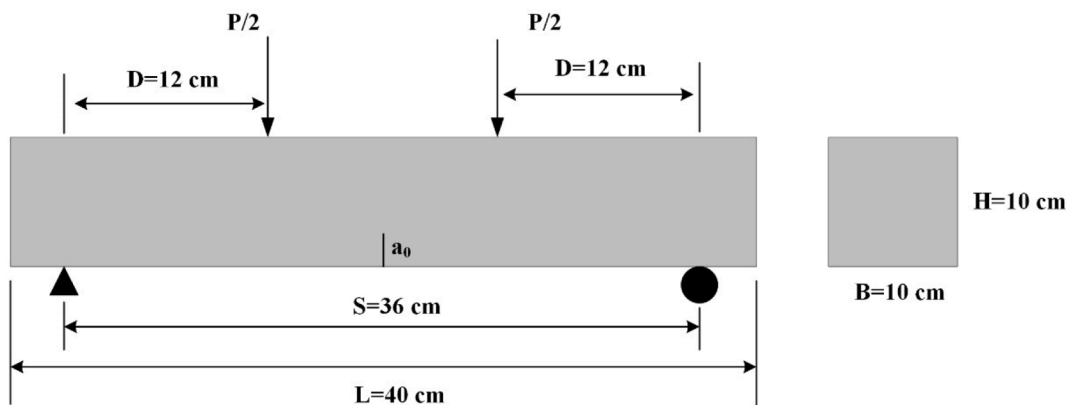
(A)



(B)



(C)



(D)

Fig. 4. Four point bending test setup for concrete specimens A) The whole setup B) the connection of LVDT for measure of mid span deflection C) the connection of LVDT for measure of CMOD D) the schematic of four point bending test and related dimensions.

retrofitting layers. Then, an YSH-90 carbon prepreg layer was added as a sensor layer. Finally, another S-glass prepreg layer was applied on top as a visual detector for damage in the YSH-90 carbon layer. The thickness of all retrofitted layers was 1 mm. After lamination, all specimens were placed on an aluminum plate, fully vacuum-sealed, and then cured in an autoclave. The epoxy resin system used in both prepreg was Hexply@913. According to the data sheet [31] for this epoxy system, the specimens were cured at 125 degrees Celsius for 60 minutes. Fig. 3 illustrates the retrofitting process with composites: lamination (Fig. 3-A), sequence of hybrid composite layers (Fig. 3-B), vacuum and autoclave

curing process (Fig. 3-C), unmolding and cleaning after curing (Fig. 3-D).

4. Four-point bending test

Fig. 4-A depicts the four-point bending test setup. The setup includes a rigid support beam, two supporting rollers, two loading rollers, a loading beam, and a hinge to ensure that the load is applied parallel to the loaded face of the prism. All rollers are aligned parallel, with a distance of 360 mm between the supporting rollers and 120 mm

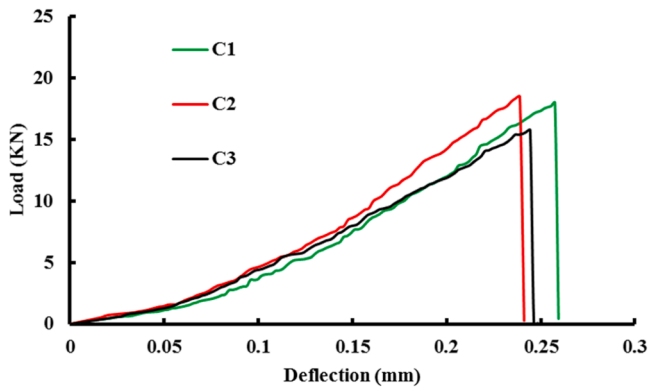


Fig. 5. the load-deflection curves for reference specimens.

between the loading rollers, which is also their distance from the nearest supporting roller. The specimen was placed symmetrically in the setup, centered, with the longitudinal axis of the prism perpendicular to the longitudinal axes of the rollers.

Deflection at the center of the prism, where the maximum displacement is expected, was measured using a linear variable differential transducer (LVDT) mounted on the lateral face at mid-span. The connection of the LVDT to the prism was carefully designed and executed. The LVDT was attached to an aluminum ruler (Fig. 4-B), which was connected to the prism with two pins at the ends. This setup prevented translation of the ruler in all three primary directions while allowing it to rotate around one pin, with the other end free to move longitudinally. This configuration ensured that the ruler, serving as the LVDT base, remained stable without restricting the prism's rotation on the supporting rollers.

For specimens with an initial crack, the crack mouth opening displacement (CMOD) was recorded using LVDT sensors (Fig. 4-C). Fig. 4-D schematically shows the dimensions of the four-point bending test setup. To create initial damage, a 2 mm wide notch was cut across the thickness of the specimens using a diamond grinding disk. The crack lengths were 5 mm and 15 mm, representing 5 % and 15 % of the cross-sectional area, respectively. The prisms were cast from normal weight concrete with a relatively high compressive strength of 68 MPa, as determined by testing cubic samples. A displacement-controlled loading protocol with a constant rate of 0.005 mm/s was used to apply the flexural load using a universal testing machine with a 200 kN load capacity.

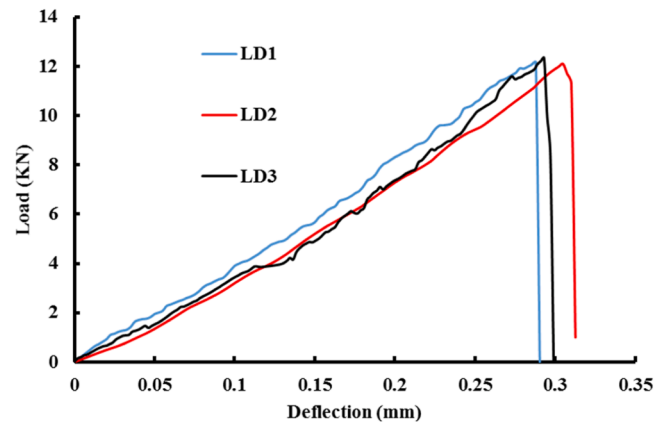
5. Results and discussion

5.1. Load-deflection curves

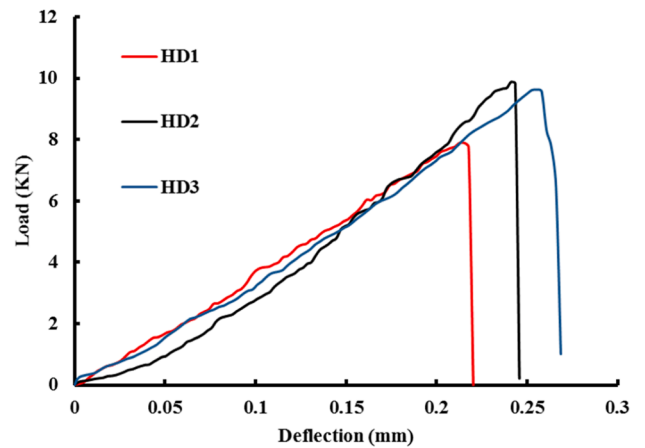
In this section, the load-deflection curves of all specimens are analyzed together. The maximum load capacity and maximum deflection values are determined for each type of specimen. Fig. 5 presents the load-deflection curves for the reference specimens. The mechanical behavior, including stiffness and maximum load (F_{max}), is consistent across the specimens. The average maximum load and deflection values for this group are 17.43 kN and 0.246 mm, respectively. To validate the maximum load value of 17.43 kN, a theoretical method was applied. The maximum load in the four-point bending test was calculated using the following equations. The theoretical calculation yielded a maximum load of 18.88 kN, indicating a 7.7 % error between the theoretical and experimental results.

$$\sigma_{ten} = \frac{MC}{I} \tag{1}$$

$$M = \frac{P}{2}D = \frac{P}{2} * 120 = 60P \tag{2}$$



(A)



(B)

Fig. 6. the load-deflection curves for A) light damage B) Heavy Damage specimens.

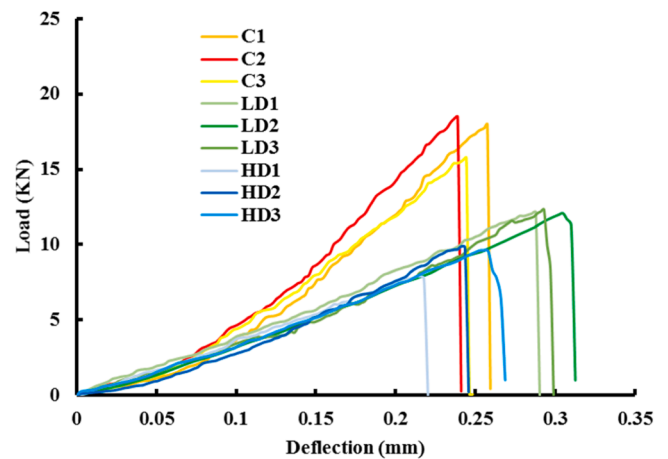


Fig. 7. Comparative of load-deflection curves for reference and damaged specimens.

$$\sigma_{ten} \approx \frac{1}{10}\sigma_c = \frac{1}{10} * 68 = 6.8Mpa \tag{3}$$

Fig. 6 illustrates the load-deflection curves for specimens with 5 percent (Figs. 6-A) and 15 percent (Fig. 6-B) damage. It is evident that the maximum load capacity for specimens with Heavy Damage is lower compared to those with Light Damage. The average maximum loads for

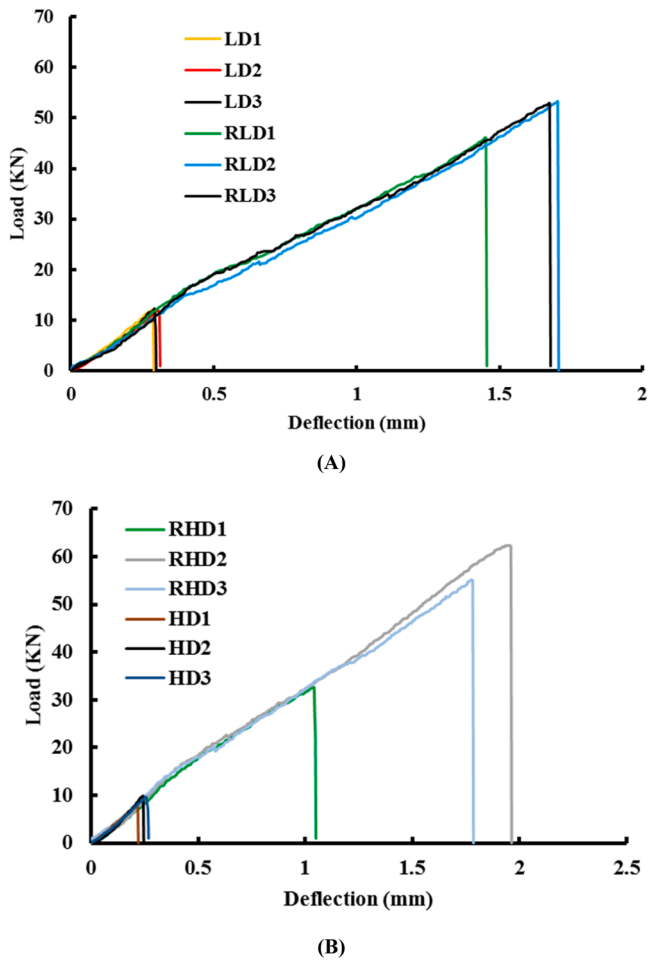


Fig. 8. The load-deflection curves for A) Retrofitted light damage and B) Retrofitted heavy damage specimens.

Table 2
The results of the tests.

Group	specimen	F _{max} (kN)	Deflection (δ _{max}) (mm)	Average F _{max}	Average δ _{max}
REF	C1	18.01	0.257	17.43	0.246
	C2	18.50	0.238	± 1.43	± 0.009
	C3	15.81	0.244		
5 % damage	LD1	12.15	0.287	12.18	0.293
	LD2	12.08	0.301	± 0.12	± 0.007
	LD3	12.33	0.293		
15 % damage	HD1	7.87	0.212	9.10	0.237
	HD2	9.88	0.241	± 1.08	± 0.024
	HD3	9.57	0.260		
Retrofitted 5 % damage	RLD1	46.10	1.445	50.76	1.603
	RLD2	53.27	1.703	± 4.04	± 0.138
	RLD3	52.92	1.661		
Retrofitted 15 % damage	RHD1	32.62	1.041	50.03	1.592
	RHD2	62.34	1.960	± 15.5	± 0.486
	RHD3	55.13	1.777		

specimens with light damage (LD) and heavy damage (HD) are 12.18 kN and 9.10 kN, respectively. These values are significantly lower than the 17.43 kN load capacity observed in the reference specimens. To compare the load-deflection behavior, particularly the slope of the curves, the graphs for all three groups were plotted in Fig. 7. As shown in the figure, the stiffness of the reference specimens is significantly greater than that of the damaged ones. This is expected, as damage typically leads to a reduction in structural stiffness. Additionally, there is no significant difference in stiffness between the LD and HD specimens,

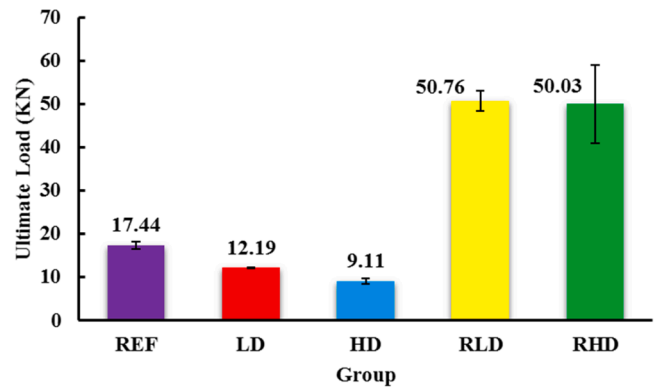


Fig. 9. Visual representation of the average ultimate loads.

although the deflection in the LD specimens is greater than in the HD specimens. The average deflection at the failure point, for the Ref, LD, and HD specimens, is 0.246, 0.293, and 0.237 mm, respectively.

Fig. 8 illustrates the load-deflection behavior of retrofitted light damage (RLD) and retrofitted heavy damage (RHD) specimens. It is evident that both the maximum load capacity and the corresponding mid-span deflection have significantly increased in the retrofitted specimens. To compare the variation in the curves between retrofitted and non-retrofitted samples, both graphs were plotted together. The average maximum load for the RLD and RHD samples is 50.73 and 50.03 kN, respectively, indicating a 416 % and 550 % increase in load capacity with the addition of just a 1 mm thick layer of hybrid composite material.

Table 2 offers a detailed summary of the test results, showing the maximum load values and corresponding deflections for all specimens. The data indicates that the depth of pre-fabricated cracks does not significantly impact the ultimate load and corresponding deflection in the retrofitted groups.

The comparison of the ultimate loads for different groups can be seen visually together in Fig. 9, where the average value for the REF group is 17.43 kN. It can be observed that a 5 mm deep crack (the LD group) reduced the load-bearing capacity by 30 % in average and a crack with a depth 15 mm (HD group) decreased the load-bearing capacity up to 48 %. On the other hand, retrofitting the damaged specimens by mechanochromic composite improves the load-bearing capacity by 208 % and 204 % for RLD and RHD groups, respectively, compared to the REF (non-damaged) group. What is interesting in this regard is that the level of pre-damage (the depth of the crack) doesn't have a significant influence on the load-bearing capacity once the prism is retrofitted with the mechanochromic composite.

Focusing on the retrofitted specimens, it is evident that the load-deflection curves exhibit a change in stiffness. To illustrate this, the load-deflection graph for the RLD3 specimen is shown again in Fig. 10. The curve can be divided into two distinct regions. In the first region, the curve's stiffness is high and matches that of the LD3 specimen. However, as the load increases beyond that of LD3, the slope of the curve changes, and in the second region, the curve exhibits a lower stiffness compared to the first region. During the test, a digital camera was positioned beneath the specimens to capture the color changes in the sensor layer of the retrofitted hybrid composite. The camera images clearly show that there is no damage at point 1, but the color of the composite surface changed (indicated by yellow bevels) at point 2. This suggests that the composite laminates at point 2 were subjected to load and experienced strain. At this point, load transfer occurs between the concrete and the composite laminates, resulting in a change in stiffness. As the load increases, the area of color change expands (as seen at points 3 and 4). It is important to note that this color change indicates damage in the high-modulus carbon layer, which has low strain-to-failure properties. The extent of damage in this layer reflects the strain level in the composite

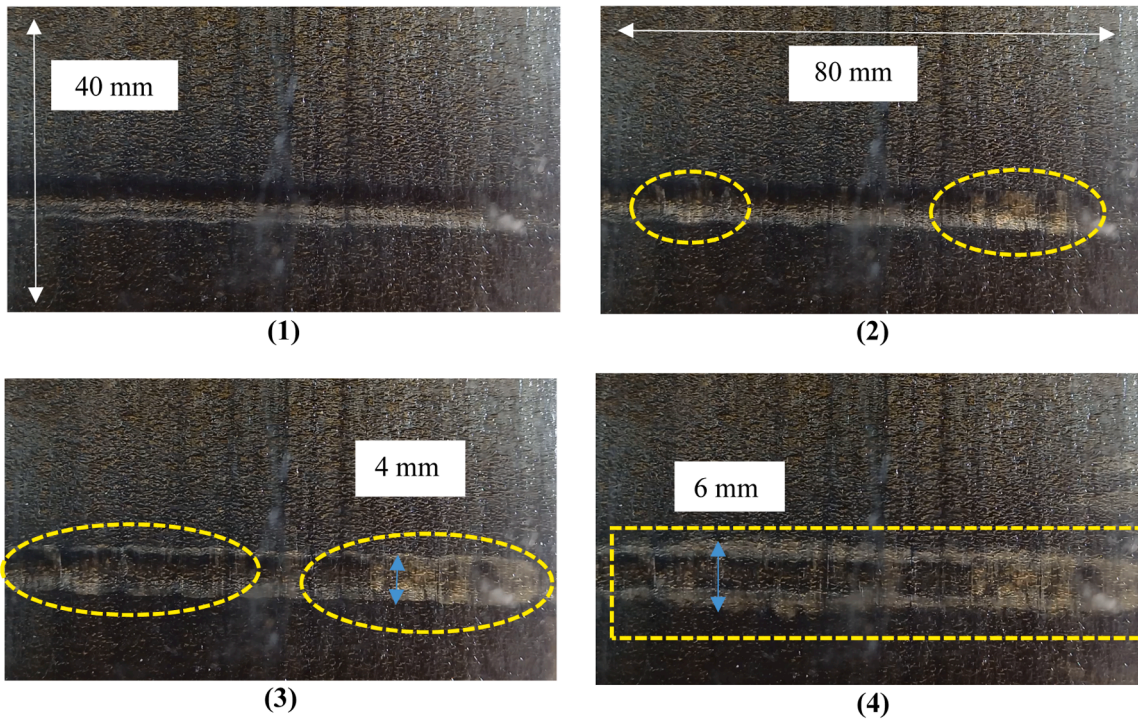
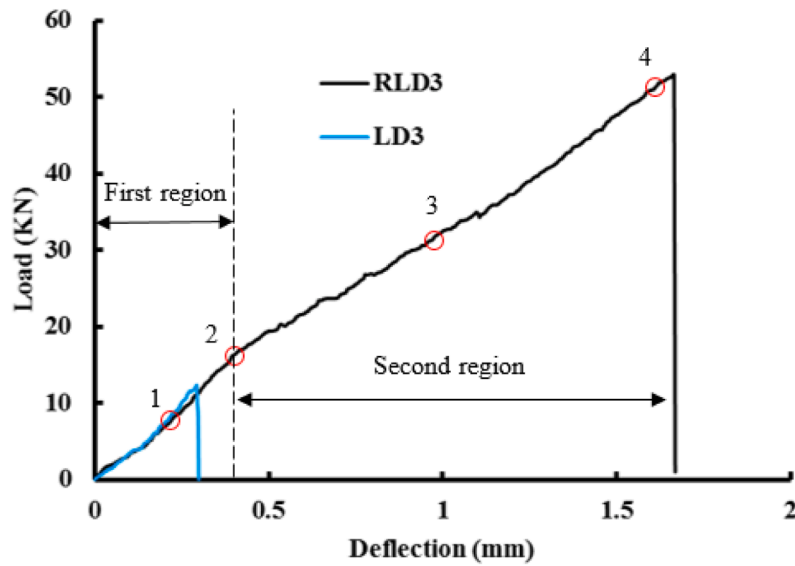


Fig. 10. Color change in the sensor of composite laminates shows the variation of load deflection curves in RLD3 specimens.

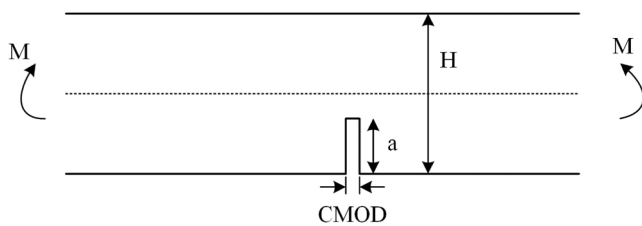


Fig. 11. The main parameters of specimens to calculate the fracture toughness in four point bending test.

layers. However, this does not imply that there is damage in the underlying S-glass layers. In fact, even after point 4, no damage has occurred in the retrofitted composite layers in this area.

5.2. Fracture parameters

In this section the stress intensity factor and fracture toughness of damaged specimens (LD1, LD2, LD3 and HD1, HD2, HD3) is calculated. The pure bending condition in the 4-point bending setup is applied around the initial notch (Fig. 11). Accordingly, to calculate the fracture toughness, the following equations (Eqs. 7–9) were used [32–34].

$$k_I = \sigma \sqrt{\pi a} F\left(\frac{a}{H}\right) \tag{7}$$

$$\sigma = \frac{3PD}{BH^2} \tag{8}$$

$$F\left(\frac{a}{H}\right) = 1.122 - 1.4\left(\frac{a}{H}\right) + 7.33\left(\frac{a}{H}\right)^2 - 13.08\left(\frac{a}{H}\right)^3 + 14\left(\frac{a}{H}\right)^4 \tag{9}$$

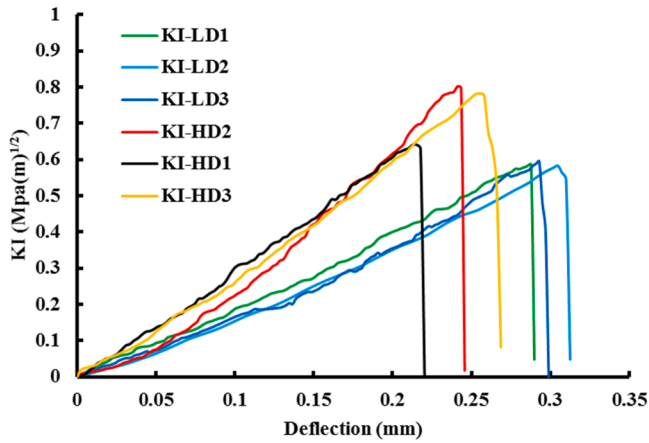


Fig. 12. The stress intensity curves of damaged specimens.

Table 3
The fracture parameters of damaged specimens.

specimen	a/H	F_{max} (KN)	K_{IC} ($MPa \cdot m^{1/2}$)	$CMOD_C$ (mm)	Average K_{IC}	Average $CMOD_C$
LD1	0.05	12.15	0.586	0.012	0.587	0.015
LD2	0.05	12.08	0.582	0.015	± 0.006	± 0.003
LD3	0.05	12.33	0.594	0.019		
HD1	0.15	7.87	0.640	0.027	0.741	0.028
HD2	0.15	9.88	0.802	0.031	± 0.088	± 0.002
HD3	0.15	9.57	0.782	0.029		

Fig. 12 illustrates the variation of the stress intensity factor (KI) for all pre-damaged specimens, with the maximum value defined as the fracture toughness (K_{IC}). Table 3 presents the fracture parameters, including maximum load, fracture toughness, and crack mouth opening displacement at maximum load ($CMOD_C$). It should be mentioned, in the retrofitted specimens, crack propagation did not occur, so fracture parameters were not calculated for these specimens. As shown in Table 3, the measured $CMOD_C$ values are 0.015 mm for light damage and 0.028 mm for heavy damage. An increase in the initial notch length results in a corresponding increase in the $CMOD_C$ parameters.

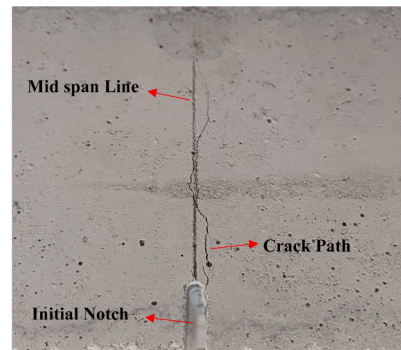
5.3. Failure modes

As seen in Fig. 13 A-D, all the specimens from non-retrofitted groups experience a common flexural failure pattern occurring in the mid-span of the prism, initiated from the tension face and progressing into the compression face until the complete failure and splitting the prism into halves. Fig. 13-A illustrates the failure mode of the reference sample without an initial damage, which fractured nearly at the midpoint under the tensile loading. Figs. 13-B and 13-C shows the failure modes of the samples with the initial damage of 5 mm and 15 mm, respectively. In these cases, the fracture initiated at the crack tip due to stress concentration and propagated almost linearly to the edge. Fig. 13-D shows the fractured surface of the HD1 specimen, where the failure surface runs parallel to the initial crack surface, with the distribution of sand and gravel particles clearly visible.

However, the retrofitted prisms demonstrated different failure mode and they failed under shear which is originated from the end of the composite layer and near one of the supports on the tension face, towards the nearest loading roller on the compression face (Fig. 14-A&B) with an approximate angle of 45 degrees. Reinforced concrete beams experience two primary types of failure: flexural failure and shear



A) C1



C) HD1



B) LD1



D) HD1

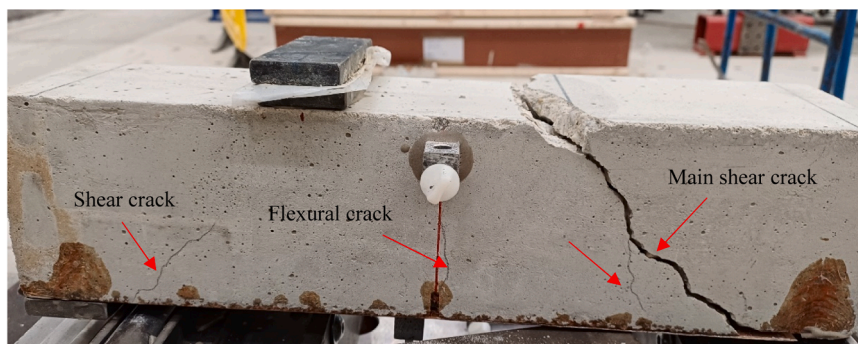
Fig. 13. The common failure mode (flexural failure) in non retrofitted specimens: A) without damage (C1) B) Light damage (LD1) C) Heavy damage (HD1) D) Cross section of HD1.



A)



B)



C)

Fig. 14. The shear failure mode in retrofitted specimens A) RLD3 and B&C) RHD2.

failure. Flexural failure happens when the applied load surpasses the beam's flexural strength, while shear failure occurs due to insufficient shear resistance between the beam's materials [21].

Fig. 15 schematically illustrates the mechanism of shear failure in the retrofitted specimens. As shown in Fig. 15-A, a series of minor flexural cracks initially formed due to stress concentration at the tip of the initial notch. As the loading progressed, these minor cracks continued to develop, with some merging into macro cracks (Fig. 15-B). As the

applied load increased, the composite bonded to the tension surface of the concrete beam began to restrict the propagation of macro cracks, which in turn reduced the stress concentration at the notch tip. However, the shear stress at the interface between the concrete beam and the composite layer steadily increased as the load on the beam continued to rise. In the following, shear minor cracks were generated on the composite part because of the stress concentration in the free edge. These micro cracks were extend along 45-degree angle. The macro cracks

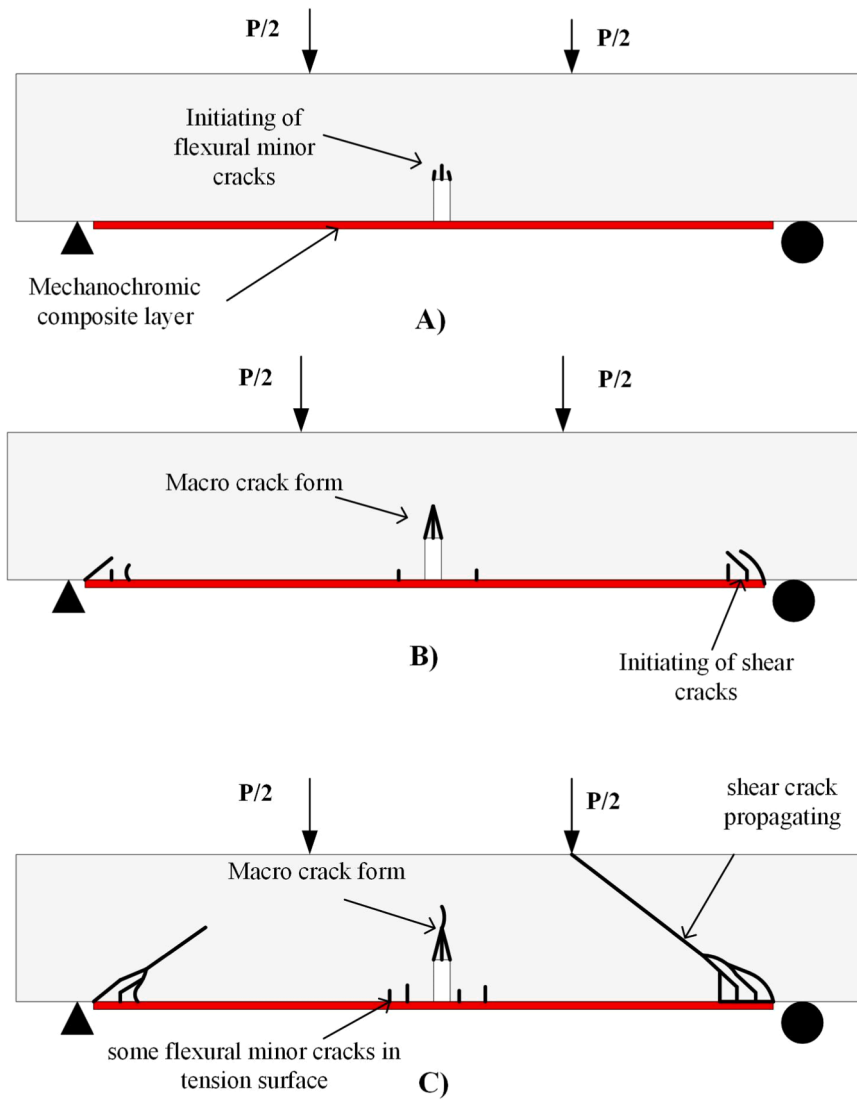


Fig. 15. The schematic of shear failure mechanism in hybrid composite retrofitted concrete beam.

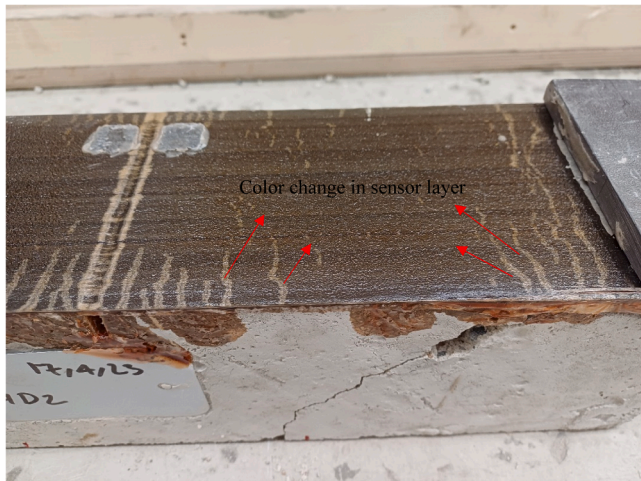


Fig. 16. Color change in the composite of a retrofitted prism, indicating a flexural cracks in concrete.

(shear cracks) developed rapidly towards the direction of the 45-degree

angle until the beam was fractured (Fig. 15-C). Additionally, the coalescence of microcracks at the ends of the composite layers leads to delamination between the composite and the concrete (see Fig. 14-A).

Although the failure primarily occurs in the concrete, the behavior of the mechanochromic composite and its color change at different stages of loading is significant. The color intensity increases as the load progresses, with notable changes occurring near collapse. Fig. 16 demonstrates the activation of the composite's self-reporting feature in response to the applied load. These color changes indicate the formation of flexural cracks on the tension surface of concrete (As discussed in Figs. 14-C and 15-C). This feature, which can be further optimized for improved visibility and sensitivity in various applications, offers valuable insight into the structural performance, serving as a passive indicator of stress accumulation, micro crack on the concrete surface and potential failure. This innovative approach can be employ as structural health monitoring (SHM) method to enhance the safety and durability of retrofitted concrete structures.

6. Conclusions

In this study, the influence of different levels of damage on the flexural behaviour of concrete prisms was investigated. Then another series of specimens with a similar level of damage were retrofitted using

an innovative self-reporting mechanochromic composite and subjected to a four-point bending test to explore the applicability of mechanochromic composites for retrofitting purposes and their impact on the structural behaviour, including load-bearing capacity, load-deflection of concrete beams and failure mode. The key findings of this study are:

- A crack with a depth of 5 % of the cross-sectional depth can decrease the load-bearing capacity up to 30 % and this reduction can reach 48 % in case the depth of the crack increases to 15 %. However, using mechanochromic composites to retrofit the damaged beams can recover the load-bearing capacity and improve it up to around 208 % comparing to a non-damaged beam, regardless of the level of the damage.
- The design of the mechanochromic composite can be adjusted for specific strengthening and health monitoring purposes by optimizing the composition and the number of layers of the composite material to: (a) achieve a desired level of enhancement in the load-bearing capacity; (b) better control over the failure mode and ductility; and (c) improvement in the clarity and visibility of the warnings offered by the composite during loading stages.
- The color changing feature of the mechanochromic composite can be helpful in monitoring the structural responses, allowing a real-time observation of damage progression and load distribution. Therefore, this innovative and cost-effective approach to SHM indicates great potential to enhance the safety and durability of civil infrastructures.

CRedit authorship contribution statement

Reza Mohammadi: Writing – review & editing, Writing – original draft, Methodology, Investigation, Conceptualization. **Ahmad Fathi:** Writing – review & editing, Writing – original draft, Methodology, Investigation, Conceptualization. **Erik Schlangen:** Writing – review & editing, Supervision. **Mohammad Fotouhi:** Writing – review & editing, Supervision, Funding acquisition, Conceptualization.

Declaration of Competing Interest

The authors declare that they have no known competing financial interests or personal relationships that could have appeared to influence the work reported in this paper.

Acknowledgement

The research presented in this paper was financially supported by the UK Engineering and Physical Sciences Research Council (EPSRC) Grants EP/V009451/1, which focused on the development of high-performance impact-resistant composites with visible damage. This work was partly financed by FCT / MCTES through national funds (PIDDAC) under the R&D Unit Institute for Sustainability and Innovation in Structural Engineering (ISISE), under reference UIDB / 04029/2020 (doi.org/10.54499/UIDB/04029/2020), and under the Associate Laboratory Advanced Production and Intelligent Systems ARISE under reference LA/P/0112/2020.

CRedit author statement

Reza Mohammadi: Conceptualization, Methodology, Investigation, Writing – original draft preparation, review & editing. **Ahmad Fathi:** Conceptualization, Methodology, Investigation, Writing – original draft preparation, review & editing. **Erik Schlangen:** Writing – review & editing, Supervision. **Mohammad Fotouhi:** Conceptualization, Funding acquisition, Supervision, Writing – review & editing.

Conflict of interest

The corresponding author confirms on behalf of all authors that there have been no involvements that might raise the question of bias in the work reported or in the conclusions, implications, or opinions stated. Furthermore, the corresponding author confirms on behalf of all authors that this material or similar material has not been and will not be submitted to or published in any other publication before its appearance in Construction and Building Materials.

Data Availability

Data will be made available on request.

References

- [1] E. Karam, R. Hawileh, T. El Maaddawy, J. Abdalla, Experimental investigations of repair of pre-damaged steel-concrete composite beams using CFRP laminates and mechanical anchors, *Thin-Walled Struct.* 112 (2017) 107–117.
- [2] Y. Yan, Y. Lu, Q. Zhao, S. Li, Flexural behavior of pre-damaged and repaired reinforced concrete beams with carbon fiber reinforced polymer grid and engineered cementitious composite, *Eng. Struct.* 277 (2023) 115390.
- [3] Y. Wang, X. Ma, J. Chen, X. Zhai, X. Zhi, H. Zhou, et al., Experimental and analytical studies on impact behaviours of a steel–concrete–steel sandwich beam with novel interlocked angle connectors, *Thin-Walled Struct.* 181 (2022) 110089.
- [4] J. Zhang, C. Tong, L. Feng, W. Du, F. Wu, Evaluation and degradation mechanism of residual performance of RC beam after drop hammer impact, *Int. J. Impact Eng.* 169 (2022) 104335.
- [5] M. Ozturk, K. Sengun, G. Arslan, CFRP contribution to load-carrying capacity of retrofitted geopolymer concrete beams, *Structures* 48 (2023) 1391–1402.
- [6] C.O. Nwankwo, J. Mahachi, D.O. Olukanni, I. Musonda, Natural fibres and biopolymers in FRP composites for strengthening concrete structures: a mixed review, *Constr. Build. Mater.* 363 (2023) 129661.
- [7] A. Borri, G. Castori, M. Corradi, Shear behavior of masonry panels strengthened by high strength steel cords, *Constr. Build. Mater.* 25 (2011) 494–503.
- [8] E. Grande, M. Imbimbo, E. Sacco, Bond behaviour of CFRP laminates glued on clay bricks: Experimental and numerical study, *Compos. Part B: Eng.* 42 (2011) 330–340.
- [9] D. Oliveira, I. Basilio, P. Lourenco, Experimental bond behavior of FRP sheets glued on brick masonry, *J. Compos. Constr.* 15 (2010).
- [10] A. Dushimimana, J. Sena-Cruz, L. Correia, J.M. Pereira, S. Cabral-Fonseca, R. Cruz, Durability of bond between EBR-CFRP laminate and concrete after four years of natural outdoor and accelerated ageing exposures, *Constr. Build. Mater.* 427 (2024) 136213.
- [11] R. Cruz, L. Correia, S. Cabral-Fonseca, J. Sena-Cruz, Durability of bond of EBR CFRP laminates to concrete under real-time field exposure and laboratory accelerated ageing, *Constr. Build. Mater.* 377 (2023) 131047.
- [12] C. López, J.P. Firmo, J.R. Correia, C. Tiago, Fire protection systems for reinforced concrete slabs strengthened with CFRP laminates, *Constr. Build. Mater.* 47 (2013) 324–333.
- [13] M. Jalaeian Zaferani, H. Shariatmadar, Repair and retrofitting of external RC beam-to-column joints using the hybrid NSM + EBR method, *Eng. Struct.* 263 (2022) 114370.
- [14] G.-L. Wang, J.-G. Dai, Y.-L. Bai, Seismic retrofit of exterior RC beam-column joints with bonded CFRP reinforcement: an experimental study, *Compos. Struct.* 224 (2019) 111018.
- [15] C.E. Bakis, Lawrence C. Bank, V.L. Brown, E. Cosenza, J.F. Davalos, J.J. Lesko, et al., Fiber-reinforced polymer composites for construction—state-of-the-art review, *J. Compos. Constr.* 6 (2002) 73–87.
- [16] M. Calis, T. Uygunoglu, A.F. Kara, Effect of heat aging on pull-off strength of FRP epoxy bonded concrete: an experimental study and fire modelling, *Constr. Build. Mater.* 439 (2024) 137290.
- [17] A. Al-Abdwais, R. Al-Mahaidi, Bond behaviour between NSM CFRP laminate and concrete using modified cement-based adhesive, *Constr. Build. Mater.* 177 (2016) 284–292.
- [18] M. Emarca, C. Barris, M. Baena, L. Torres, J. Barros, Bond behavior of NSM CFRP laminates in concrete under sustained loading, *Constr. Build. Mater.* 177 (2018) 237–246.
- [19] N. Khodadadi, H. Roghani, E. Harati, M. Mirdarsoltany, F. De Caso, A. Nanni, Fiber-reinforced polymer (FRP) in concrete: a comprehensive survey, *Constr. Build. Mater.* 432 (2024) 136634.
- [20] L.C. Hollaway, A review of the present and future utilisation of FRP composites in the civil infrastructure with reference to their important in-service properties, *Constr. Build. Mater.* 24 (2010) 2419–2445.
- [21] S. Degala, P. Rizzo, K. Ramanathan, K.A. Harries, Acoustic emission monitoring of CFRP reinforced concrete slabs, *Constr. Build. Mater.* 23 (2009) 2016–2026.
- [22] A. Mirmiran, S. Philip, Comparison of acoustic emission activity in steel-reinforced and FRP-reinforced concrete beams, *Constr. Build. Mater.* 14 (2000) 299–310.
- [23] S. Sasmal, S. Basu, C.V.V. Himakar, T. Kundu, Detection of interface flaws in Concrete-FRP composite structures using linear and nonlinear ultrasonics based techniques, *Ultrasonics* 132 (2023) 107007.

- [24] P. Malla, S.S. Khedmatgozar Dolati, J.D. Ortiz, A.B. Mehrabi, A. Nanni, J. Ding, Damage detection in FRP-reinforced concrete elements, *Materials* 17 (2024).
- [25] M. Yumnam, H. Gupta, D. Ghosh, J. Jaganathan, Inspection of concrete structures externally reinforced with FRP composites using active infrared thermography: a review, *Constr. Build. Mater.* 310 (2021) 125265.
- [26] A. Tabatabaeian, R. Mohammadi, P. Harrison, M. Fotouhi, Characterisation and application of bio-inspired hybrid composite sensors for detecting barely visible damage under out-of-plane loadings, *Sensors* 24 (2024).
- [27] A. Tabatabaeian, S. Liu, P. Harrison, E. Schlangen, M. Fotouhi, A review on self-reporting mechanochromic composites: An emerging technology for structural health monitoring, *Compos. Part A: Appl. Sci. Manuf.* 163 (2022) 107236.
- [28] M. Jalalvand, G. Czél, M.R. Wisnom, Damage analysis of pseudo-ductile thin-ply UD hybrid composites – a new analytical method, *Compos. Part A: Appl. Sci. Manuf.* 69 (2015) 83–93.
- [29] M. Jalalvand, H. Wu, F. Sheibanian, M. Fotouhi, M. Wisnom, Self-Warn. Hybrid. Compos. patches Repair. Crack. Alum. Panels (2018).
- [30] M. Fotouhi, M. Jalalvand, M.R. Wisnom, High performance quasi-isotropic thin-ply carbon/glass hybrid composites with pseudo-ductile behaviour in all fibre orientations, *Compos. Sci. Technol.* 152 (2017) 101–110.
- [31] HexPly® 913 Epoxy matrix (125°C curing matrix) HCP.
- [32] H. Tada, P.C. Paris, G.R. Irwin, *The Stress Analysis of CRACKS Handbook*. New York, USA, ASME Press, 2000.
- [33] S. Xu, H.W. Reinhardt, Determination of double-K criterion for crack propagation in quasi-brittle fracture, Part II: analytical evaluating and practical measuring methods for three-point bending notched beams, *Int. J. Fract.* 98 (1999) 151–177.
- [34] Y. Yin, Y. Qiao, S. Hu, Four-point bending tests for the fracture properties of concrete, *Eng. Fract. Mech.* 211 (2019) 371–381.